Thermochimica Acta 482 (2009) 1–7

Contents lists available at ScienceDirect

Thermochimica Acta

journal homepage: www.elsevier.com/locate/tca

# Calorimetric measurements of undercooling in single micron sized SnAgCu particles in a wide range of cooling rates

Y.L. Gao[a,*], E. Zhuravlev[b], C.D. Zou[a], B. Yang[a], Q.J. Zhai[a], C. Schick[b]

[a] Shanghai Key Laboratory of Modern Metallurgy and Materials Processing, Shanghai University, Shanghai 200072, PR China
[b] Institute of Physics, University of Rostock, Universitätsplatz 3, 18051 Rostock, Germany

ARTICLE INFO

*Article history:*
Received 15 June 2008
Received in revised form
29 September 2008
Accepted 1 October 2008
Available online 17 October 2008

*Keywords:*
Undercooling
Cooling rate
Fast scanning chip calorimeter
Single metal particle

ABSTRACT

A fast scanning chip-based calorimeter was applied for the measurement of single micron sized particles. The cooling rate dependence of undercooling was studied for Sn–3.0Ag–0.5Cu (wt.%) alloy particles. Combining DSC and fast scanning chip calorimetry, the cooling rate covers six orders of magnitude. For the single particles under investigation average undercooling ranges from about 30 K at 0.025 K/s to 120 K at $10^4$ K/s. After several hundred heating–cooling cycles the single particles remain spherical and do not wet the sensor surface. The data points at one rate are highly scattered due to the stochastic nature of the nucleation event. The newly developed fast scanning calorimeter opens up a possibility to study not only cooling rate but also size dependency of undercooling of single micron and sub-micron sized particles. In future, this technique will allow a comparison between theoretical estimates and experimental data. In this paper we demonstrate the possibility of single particle measurements in a wide range of cooling rates. We focus on the experimental challenges of such experiments like calibration, heat transfer limitations, and sample placement on the sensor. Furthermore we discuss problems arising from the significantly enlarged heat exchanging area, when adding a 50 μm spherical particle to the calorimeter membrane.



## 1. Introduction

The undercooling, which depends on nucleation and crystal growth, is one of the significant factors affecting the structure of metallic materials and the ultimate material properties [1–3]. Novel materials with refined structure and superior properties will be usually developed by controlling their solidification process. Decreasing droplet size influences undercooling and consequently the whole solidification process [4,5]. Beside particle size another crucial factor for the solidification process is cooling rate. As long as ensembles of particles are needed for the measurement of undercooling, due to decreasing signal to noise ratio for smaller single particles, it is challenging to distinguish between cooling rate and particle size influence. Nevertheless, some attempts are known to distinguish the separate influence of particle size and cooling rate [6,7]. Knowledge gained about the influence of cooling rate from these studies was limited due to the small cooling rate range accessible. Therefore, studies in a wider cooling rate range are of interest in order to distinguish the influences of cooling rate and particle size. So far mainly DTA and DSC were utilized for the measurement of undercooling for metallic materials [8–10]. Commonly ensembles of particles are studied and particle size distributions have to be considered [7,11].

Measuring solidification of single micron sized metal particles seems to be an attractive alternative to overcome some of the problems of the DSC methods [12]. With the development of chip based thin film calorimeters measurements on nanogram samples became possible recently [13,14]. The first attempts were focused on adiabatic conditions and therefore limited to heating. At non-adiabatic conditions thin film calorimeters allow controlled fast cooling too [15–18]. Therefore we employed this technique for a study of undercooling of single micron sized metal particles in a wide range of cooling rates.

The Sn–3.0Ag–0.5Cu (wt.%) alloy system is considered as one of the substitutes to replace Pb-containing solders [19]. Single particles made of this alloy were chosen for the calorimetric measurements because of its appropriate low melting temperature. The particles were highly stable in shape because of the missing reactivity and poor wettability of SnAgCu with the sensor surface ($SiO_2$). Consequently, the cooling rate dependence of undercooling of single micron sized spherical SnAgCu particles could be investigated in a wide range of cooling rates.

* Corresponding author.
*E-mail address:* gaoyulai@163.com (Y.L. Gao).

0040-6031/$ – see front matter © 2008 Elsevier B.V. All rights reserved.
doi:10.1016/j.tca.2008.10.002

## 2. Experimental

### 2.1. Calorimetric measurements

Conventional DSC is one of the few techniques that have a large dynamic range in relation to heating and cooling rates varying from (quasi) isothermal measurements to measurements at rates up to 8 K/s [20]. For a power compensated DSC (PerkinElmer Pyris Diamond HyperDSC™ was used here) these rates are available on heating as well as on cooling. Higher rates are not possible because of the thermal inertia of the measuring cell. Several approaches are known to overcome these limitations. Most of them are based on thin film techniques. Quasi-adiabatic scanning calorimetry at high heating rates, ca. 500 K/s, was developed by Hager [21] and for rates up to $10^7$ K/s, by Allen and co-workers [13,22]. But for studying solidification fast cooling is essential.

Fast scanning non-adiabatic nanocalorimetry based on thin film chip sensors with extremely small measuring area extends scanning rate range at cooling significantly. Non-adiabatic conditions are realized by operating the sensor in a gas rather than in vacuum. For the sensors used in this study heat losses through the gas are larger than the losses through the 0.5 μm thick $SiN_x$ membrane [23]. Until now this is the only technique that is capable of applying both controlled heating and controlled cooling at rates up to $10^6$ K/s [15]. Unfortunately at low rates, signal to noise ratio and therefore sensitivity is dramatically reduced. Usually the device is limited to rates above $10^2$ K/s. It is a general rule for all calorimeters that using one and the same sample allows to obtain reliable data only in a restricted scanning rate interval [20]. That is because heat flow given to or taken from the sample on heating or cooling, respectively, scales with rate and causes serious thermal lag at higher rates for larger samples, see below, or bad signal to noise ratios at low rates.

In order to bridge the gap between HyperDSC™ (<8 K/s) and ultra fast scanning (>100 K/s) a new device was developed. It is based on the same type of chips as used in [15,16,24] connected in a differential scheme with power compensation (Fig. 2). It allows both heating and cooling with rates from 1 to $10^4$ K/s. This interval was of particular interest for the solidification of single alloy particles because it covers the technologically relevant range of cooling rates for common and rapid solidification processes of metals.

The fast scanning calorimeter uses a high sensitive, low addenda heat capacity thin film sensor (XI-296 [15,16,24]). It consists of a Si frame 2.5 mm × 5 mm fixed on a standard integrated circuit housing. The actual calorimeter consists of a heater and a thermopile embedded at the center of a 0.5 μm thick freestanding $SiN_x$ membrane, see Fig. 1(A) and (B). The size of the heated area is about 60 μm × 80 μm. A high sensitive semiconducting thermopile is placed inside this area: consisting of 6 "hot" junctions in the center and 6 "cold" junctions on the frame (dark green, color online), see Fig. 1(C) and (D). For fast scanning experiments the sample must be placed inside the heated area. Then reliable information about sample temperature for thin samples can be obtained. Otherwise the strong temperature gradient outside the heated area influences the measurement [25] and uncertainty of temperature measurement increases dramatically. The temperature profile inside the heater area (60 μm × 80 μm) is basically homogeneous [25]. The experimental results shown in [25] and modeling using an analytical model of the membrane gas system [23] show that temperature differences between the central part of the heater stripes to the center of the measurement area are commonly in the range of a few Kelvin. These results were further confirmed [26] by optical studies of the nematic to isotropic transition of the liquid crystal HP 53 [27]. To ensure correct temperature measurements on fast scanning the single particle must be positioned in the center of the

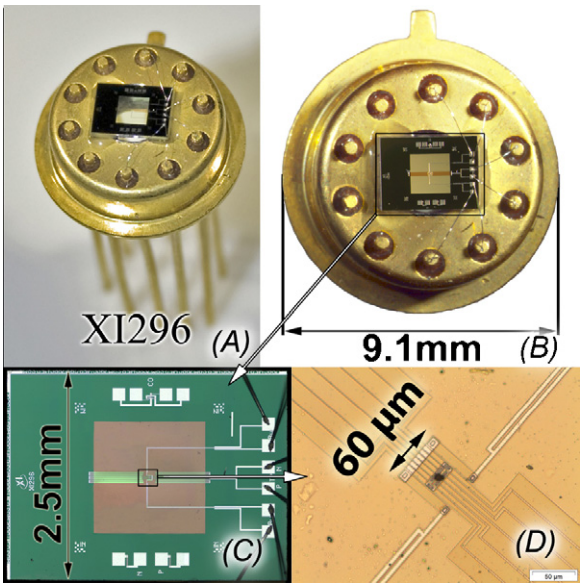


**Fig. 1.** Measuring cell of the calorimeter. Xensor Integration gauge XI296 [24]. (A) and (B) show the whole sensor, (C) the silicon frame and (D) the heated area on the freestanding membrane in the center of the chip.

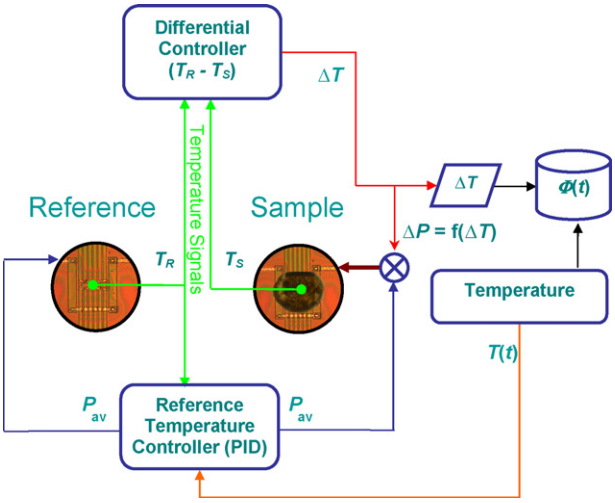


**Fig. 2.** Scheme of the differential setup with power compensation, for details see text.

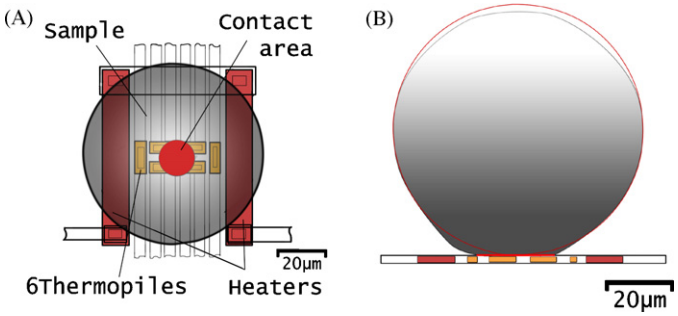


**Fig. 3.** Sample placement on the sensor: (A) Top view indicating the small contact area between the spherical sample and the senor. (B) Side view showing the small deformation of the sample after several heating–cooling cycles.

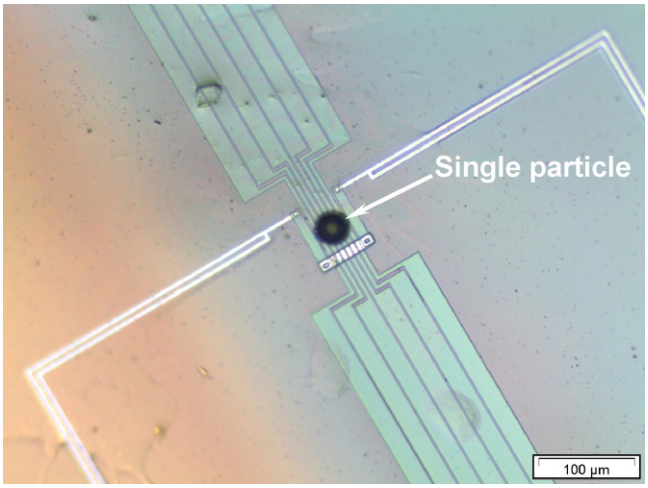


**Fig. 4.** Microphotograph (Olympus BX 41) of a single particle positioned in the measuring area of the sensor for fast calorimetric measurements.

heated area and must be in direct contact with the thermopile hot junctions, as shown in Figs. 3 and 4.

The basic principle of the power compensated differential fast scanning chip calorimeter follows with a slight modification the power compensation scheme realized by PerkinElmer Inc. [28,29]. Instead of cups with mass of more than 1 g it consists of two thin film sensors (XI-296 [24]) mentioned above. Two of the sensors are connected in a differential setup. One is loaded with the sample and the other is empty.

Two control circuits are used to control the temperature of the sensors. The first circuit controls the temperature of the reference sensor by means of an analog proportional–integral–differential controller (PID). The temperature of the sample sensor is not considered by this control loop. Nevertheless, the output voltage of the PID is feed to the heaters of the reference sensor as well as of the sample sensor. The second control circuit (differential controller $(T_R - T_S)$) realizes the power compensation. It compensates for any temperature difference between sample and reference sensor by adding or subtracting the appropriate voltage from the sample sensor heater voltage. This way both sensors follow the predefined temperature program very closely ($T_R - T_S < 0.1$ K) even at $10^4$ K/s and quantitative calorimetric measurements are possible as described elsewhere [26]. The power needed for this compensation yields directly the heat capacity of the sample inside the heated area as long as addenda heat capacity and losses of both sensors are the same. The necessary data for calculation of heat capacity is being collected using a fast DAQ board (Meilhaus ME4680i) at sampling rates up to 500 kHz.

The thermopile of the calorimeter was calibrated with flat indium and tin samples of about 1 μm thickness. For ideally placed samples accuracy of the temperature measurement is about ±5 K. For heat capacity and heat of fusion of the metal particles reasonable values were obtained. Measured heat of fusion decreases for about 20% between 1 K/s and $10^4$ K/s because the control electronics cannot precisely control sample sensor temperature at high rates for the large samples studied. The enthalpy change during solidification could not be determined correctly because solidification is so fast that not enough data points for peak integration were collected. Heat capacity values before melting or crystallization peaks are within ±10% in the applied scanning rate range. Therefore thermal lag corrected peak onset temperatures for melting and solidification could be determined in the common way without large perturbations due to uncertainties of the measured heat capacity as shown below.

### 2.2. Sample preparation

The eutectic master alloy with the nominal composition of Sn–3.0Ag–0.5Cu (wt.%) was prepared by induction melting, and the micro-sized particles were prepared by the consumable-electrode direct current arc (CDCA) technique [30]. For induction melting Sn, Ag and Cu with 99.9 wt.% purity was melted and intensely stirred by the magnetic field for about 10 min to obtain a homogeneous master alloy. The anode and cathode for the CDCA technique were shaped by suction casting as cylinders with diameter 6 mm and length ca. 200 mm. Particles could be prepared in various sizes from a few to hundreds of microns when an arc was produced between the two electrodes. The voltage between the two electrodes was about 20 V and the current 20 A. The CDCA process was performed in liquid paraffin as a coolant at ambient temperature to prevent oxidation of the particles. Due to surface tension and hydrostatic pressure, produced by the liquid paraffin, particles in nearly perfect spherical shape were obtained.

Single spherical particles with diameters ranging from 36 to 52 μm were measured with the fast scanning calorimeter. The micrometer sized spherical particles were placed in the center of the measuring area of the chip sensor, see Figs. 1D and Fig. 4. To improve the thermal contact between sample and membrane Apiezon™ N vacuum grease was used. After the first heating-cooling scan the grease remains as a thin (<1 μm) layer covering the sample-membrane contact area providing an improved thermal contact between sample and membrane. The part of the grease which is not bound by capillary forces between membrane and particle moves on first heating to the edge of the membrane and therefore out of the measuring area. The remaining small amount of grease does not add much, in comparison to sample heat capacity, to the addenda heat capacity. It also behaves inert and does not produce any peaks in the measured curves due to phase transitions in the temperature range of interest.

The sample must be placed in the center of the heated area of the sensor to avoid measurement errors by the steep temperature gradient outside of this area [25].

Even if the sample is placed exactly on the heated area of the sensor, the position and the thermal contact between sample and membrane will affect sample temperature measurement. This influence is twofold: (i) Thermal lag caused by the effective thermal resistance between sample and membrane influences the temperature measurement. The effective thermal resistance increases for spherical samples in comparison to flat samples due to the much smaller contact area. This small contact area also causes the second problem: (ii) If the sample is positioned not exactly on the thermopiles, the thermopile signal differs from the temperature at the contact area between sample and sensor. This is because of distortions of the temperature profile of the heated area of the sensor due to the significantly increased heat exchanging area with the environment (the gas). For the empty sensor only the two faces of the heated part of the membrane exchange heat with the gas. For the sensor with sample the area is increased by the surface area of the particle. Consequently the particle is an additional heat sink and therefore deforming the temperature profile of the membrane. This deviation is rate independent as long as quasi static conditions for the membrane–gas system are realized [15], which is always the case in this study.

The single particles for the measurements were selected with the help of an optical microscope (Olympus SZX 16). Using a soft copper wire the selected particle was positioned on the heater zone of the sensor for calorimetric measurements, see Fig. 4.

The shapes of the single particles were checked with an Olympus BX 41 Microscope before and after the calorimetric measurements. The particle remained basically spherical even after hundreds of

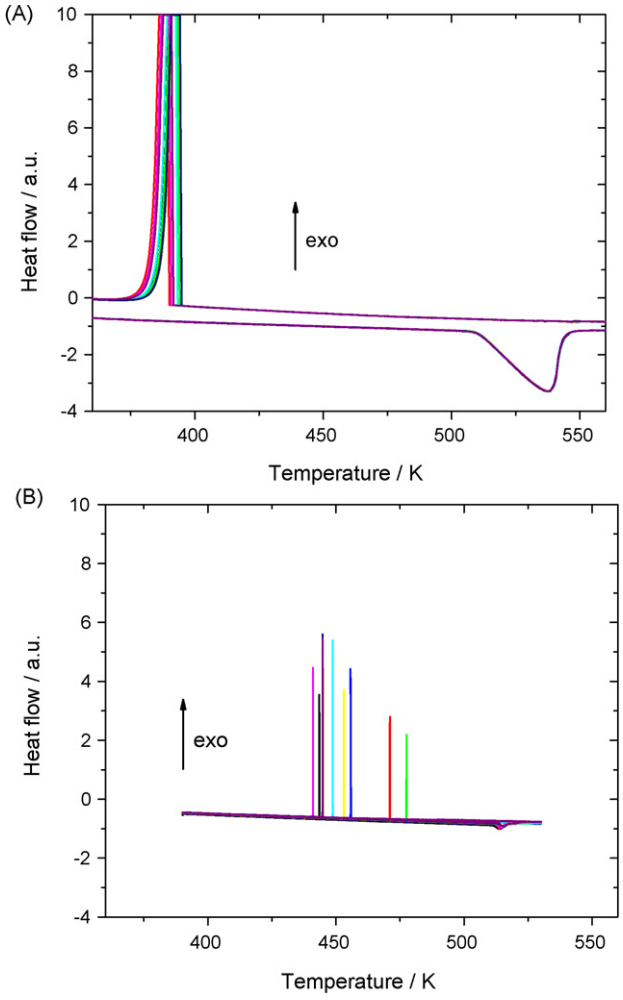


**Fig. 5.** Heating and cooling curves of the 47 μm diameter particle at cooling rate of (A) 1000 K/s and (B) 5 K/s. 10 successive heating–cooling cycles are shown.

heating–cooling cycles as applied for the fast scanning experiments. Furthermore the measured single particle could be easily removed from the sensor surface and a clean surface was obtained. Only the thin layer of Apiezon™ N vacuum grease remains on the sensor.

Five single SnAgCu particles with a diameter of 52, 47, 45, 38, and 36 μm were chosen for the undercooling investigations. Scanning rates from 1 to $10^4$ K/s were employed to study the effect of cooling rate on the undercooling of these single particles. It should be noticed that the studied particles kept their original shape and changes of particle size were not observed. Therefore, the cooling rate dependence of undercooling of each single metal particle could be investigated and was not superimposed with changes in sample geometry or size distributions.

## 3. Results

Fig. 5 shows the heating and cooling curves for 10 successive heating cooling scans of one particle. As expected the melting peaks (plotted downwards) are one on top of the other, showing the high reproducibility of the measurements. In contrary solidification temperature scatters within about 10 K at 1000 K/s cooling rate and up to 40 K at 5 K/s. The linear leading edge of the melting peak, showing a shallower slope compared to the much steeper slope of the crystallization peak, indicates a thermal resistance limited heat flow to the sample on melting as it is well known from DSC too [27,31,32]. Due to the large undercooling crystallization is a very abrupt process yielding very sharp peaks. As discussed in [33] even for 2 mm diameter particles or 80 μm Al particles [12], it can be assumed that only one nucleation event occurs and the particle solidifies immediately. We consider the same for our small particles too. So far we did not check the internal structure of the solidified particles. Therefore we do not know the crystal morphology or the detailed composition of each particle.

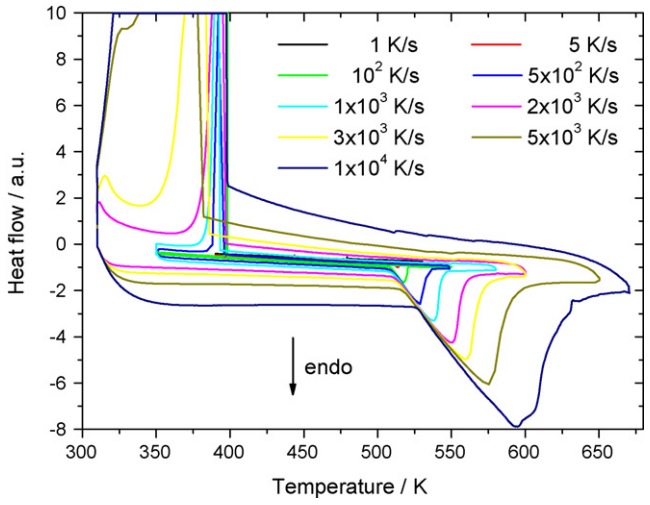


**Fig. 6.** Heating and cooling curves for different rates for the particle of 47 μm diameter. At the highest cooling rates losses to the surrounding are not high enough to allow controlled cooling at low temperatures when the sample crystallizes.

The half height width of the crystallization peak is about 10 ms. The width is mainly caused by the time constant of the system representing sample–sensor–control and measuring electronics. Nevertheless, the smearing is not important for our study because we only evaluate the crystallization onset, which is corrected for heat transfer problems as described below. Furthermore, the peak onset is not influenced by crystal growth rate. Statistics of nucleation determine the scatter of the crystallization (peak onset) temperature for the different cooling scans.

In Fig. 6 measured curves at different heating and cooling rates are shown for one single particle. As expected the leading edges of the melting peaks superimpose each other because of the thermal resistance which limits the heat flow during melting. From these curves melting onset was determined as usual [31].

Heat flow to the sample, $\Phi_s$, is limited by the effective thermal resistance, $R_{th}$, between the particle and the membrane. The resulting temperature difference $\Delta T$ (thermal lag) between sample and sensor can be expressed as

$$\Delta T = R_{th} \bullet \Phi_s \quad \text{with} \quad \Phi_s = m_S c_p \frac{dT}{dt} \tag{1}$$

where $m_S$ is sample mass, $c_p$ is specific heat capacity of the sample and $dT/dt = \beta$ is heating/cooling rate.

For metal particles in the micron range no size or rate dependence for the melting temperature is expected. According Eq. (1) thermal lag increases linearly with rate. Consequently the measured apparent melting temperature (peak onset) should also increase linearly with heating rate. Fig. 7 shows this dependency for the 47 μm diameter particle. Apparent melting points at rates above 100 K/s are lying on a straight line, confirming the validity of Eq. (1) for the case under investigation. Why the two points at the lowest rates (1 and 5 K/s) deviate from the line is not yet known.

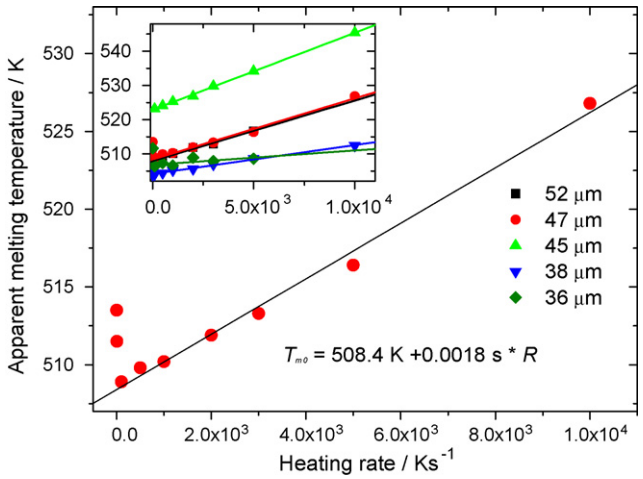


**Fig. 7.** Heating rate dependence of apparent melting temperature (peak onset) of the 47 µm diameter particle. In the inset the dependencies for all particles are shown.

From the slope of the linear fit a time constant of about 2 ms is obtained. This is a rather small value compared to common values for DSC which are of the order of 3 s. But at rates of $10^4$ K/s even this small time constant result in a temperature difference (thermal lag) of about 20 K across the effective thermal resistor between sample and membrane. The lag could be significantly reduced by enlarging the contact area between sample and sensor, e.g. using a thin flat film as a sample. For such a few micron thick flat samples thermal lag is below the detection limit of 100 µs as shown by separate measurements [26]. But this is not an option for us because we are interested in the behavior of spherical particles. As seen from Figs. 5 to 7, Eq. (1) describes the behavior of the apparent melting temperature reasonable well and we can use it to correct the measured melting and solidification temperatures for thermal lag.

For the melting peak onset temperature the heat capacity of the solid alloy determines the thermal lag, see Eq. (1). Assuming a similar value for the heat capacity of the liquid alloy thermal lag at cooling is described by Eq. (1) with the same value of $R_{th}$, $c_p$ and $m_s$ as well. Melting and crystallization temperatures were therefore corrected by Eq. (1) [31,34] assuming the same slope for heating and cooling. This way melting temperature becomes rate independent and the intersections of the straight line in Fig. 7 at heating rate zero should equal the true melting temperature of the substance under investigation. The different slopes of the curves in the inset of Fig. 7 are due to different effective thermal resistances between sample and membrane, which is reasonable for different particles. But the different intersections cannot be explained by this effect. Melting temperature of the bulk SnAgCu alloy equals 490 K and we measure intersects up to 525 K. This deviation is far outside the uncertainty of temperature calibration of the device of about ±5 K.

The following reasons may cause such large error in the temperature measurement on an absolute scale.

(i) The sample was not always placed perfectly in the center of the heated area on top of the thermopiles as shown in Figs. 3 and 4 or it had moved a little during the measurement cycle. In both cases sample temperature will be different from that indicated by the thermopile and melting temperature determined will be different too. If the sample is placed away from the heater stripe sample temperature will be lower and if the sample is closer to the heater stripe temperature will be higher, yielding higher or lower measured melting temperatures, respectively. This effect may cause differences of a few Kelvin [23,25], as discussed briefly in Section 2.1, but not the deviation of 30 K as seen in the inset of Fig. 7.

(ii) A more severe problem arises from the large surface area of the micron sized particles. For the empty sensor or a sensor loaded with a flat sample the main heat exchanging area (two surfaces) is about 10,000 µm$^2$ [15,23,25]. Placing a 50 µm diameter spherical particle on one side enlarges the total surface by about 8000 µm$^2$. This large additional heat-exchanging surface causes significantly higher heat losses into the surrounding gas. Due to the small contact area between the spherical sample and the membrane this results in a local "cooling" at the contact spot between sample and membrane. If the contact spot is not covering the thermopiles sample temperature may be significantly lower than temperature measured by the thermopile. Again, sample placement is essential for accurate absolute temperature measurements for such large spherical samples.

(iii) Beside the problems related to the calorimetric measurements the actual alloy composition of the single particle may add another uncertainty regarding the true melting temperature for each micron sized particle. Unfortunately, at the moment we do not know about deviations of the composition of the studied particles compared to the master alloy but it cannot be excluded.

In this study we are not primarily interested in absolute temperature measurements but in determining a possible rate dependence of undercooling. The effects discussed above do not depend on heating or cooling rate as long as rate is not too high. In [15] it was shown that quasi static conditions are realized for this kind of sensors up to heating and cooling rates of $10^5$ K/s for flat samples. At $10^4$ K/s, the highest rate employed here, this condition is fulfilled for the spherical particles as well.

In order to determine undercooling of solidification of single spherical SnAgCu micro particles as function of cooling rate the following procedure was applied:

- Single spherical particles were placed as perfect as possible on the thermopile in the center of the heated area of the sensor, see Fig. 4.
- Heating–cooling cycles at different rates between 1 and $10^4$ K/s were performed. For each rate 10 cycles were recorded, see Figs. 5 and 6.
- The apparent melting onset temperature $T_{measured}$ was determined for all heating rates, $\beta = dT/dt$, and plotted versus rate, see Fig. 7. The slope, $S$, of the linear fit was used to correct for thermal lag according $T_{corr} = T_{measured} - S\beta$. The same correction was applied for the apparent solidification temperature $T_{solidif}$ at cooling using negative rates.
- Undercooling for each measurement was determined as $T_{m\,corr} - T_{solidif\,corr}$ and plotted versus logarithm of cooling rate as shown in Fig. 8.

As shown in Fig. 5 undercooling at one rate for one single particle scatters largely. Especially at low rates the scatter is high. All together undercooling in our study spans from 30 to 130 K for cooling rates from 1 to $10^4$ K/s. At cooling rates between 100 and 10,000 K/s undercooling is centered around 110 K and shows a very weak cooling rate dependency. At cooling rate 1 and 5 K/s undercooling is reduced to a mean value of about 70 K.

The particles studied were all within a diameter of a few dozens of micrometers. Therefore we do not expect significant influences of particle size on undercooling and plot all data available in Fig. 9. We add some data points from DSC at lower rates which were obtained

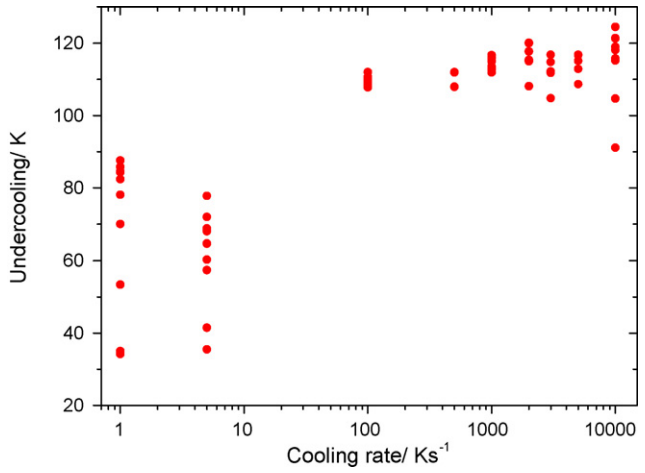


**Fig. 8.** Undercooling for one single particle of SnAgCu alloy of 47 μm diameter at different cooling rates.

in exactly the same way but for single particles with diameter larger than 500 μm.

Fig. 9 shows all data from all samples (5 samples, 10 measurements at each rate for fast scanning, plus five larger samples for DSC at 6 different rates). Again no smooth rate dependency is seen for the different particles rather than a stepwise change in undercooling with rate.

## 4. Discussion

Undercooling of single micron sized particles of the alloy Sn–3.0Ag–0.5Cu (wt.%) depends on cooling rate as shown in Fig. 9. Despite large scatter undercooling of the SnAgCu alloy single particles ranges from about 25 K at a cooling rate of 0.025 K/s (1.5 K/min) to about 135 K at a cooling rate of $10^4$ K/s. This is an extremely high undercooling for this alloy. Combining DSC and fast scanning calorimetry allows studying undercooling of single micron sized spherical particles covering 6 orders of magnitude in cooling rate. For DSC experiments particles of a few hundred micrometers diameter are needed while for the fast scanning a few micrometers are sufficient.

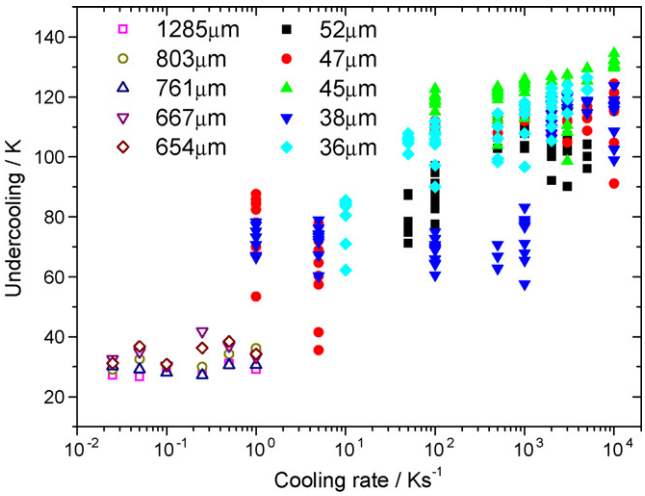


**Fig. 9.** Relation between undercooling and cooling rate for all particles studied. The solid symbols indicate the data obtained by fast scanning calorimetry and the open symbols that obtained by DSC measurements. Note: there are 400 points for fast scanning and 30 points for DSC measurements included in this figure.

The obtained data do not follow a clear trend. For one single particle undercooling changes stepwise with cooling rate. The reasons for this behavior as well as for the large scatter at one cooling rate are not yet known. Probably some impurities in the particles act as nucleation sites and depending on the thermal history these impurities may be placed differently inside the particle. Depending on the position, closer to the center or closer to the edge, nucleation may be delayed or enhanced. Unfortunately we cannot yet draw conclusions about the rate dependency of undercooling from our measurements. A detailed description of the rate dependence of undercooling requires a better understanding of the nucleation mechanism in the SnAgCu alloy particles.

Compared to other studies of pure metal particles the scatter in undercooling for the alloy particles under investigation is very large. The scatter of undercooling in single 80 μm Al droplets [12] was a few Kelvin only and centered around 45 K. A similar result was found for a single 2 mm Au particle, the undercooling scattered finally after removal of impurities for a few Kelvin around 210 K [33]. For millimeter sized droplets of Ta and Re, solidified via the Grenoble high drop tube, the undercooling was scattered within a few ten Kelvin around the mean value of 625 and 860 K, respectively, [35]. For micron sized particles of pure tin, prepared and measured in the same way as the alloy particles, preliminary experiments show an undercooling of about 100 K and a scatter of a few Kelvin only. This is in good agreement with the results mentioned above but leaves the question open why nucleation in the SnAgCu alloy particles scatters so much.

Summarizing, the newly developed fast scanning calorimetry opens up not only the possibility to study cooling rate dependence of undercooling of single micron sized particles, it also allows studying particle size dependence of undercooling.

## Acknowledgements

The work is supported by Robert Bosch Foundation (Grant no. 32.5.8003.0025.0/MA01), the National Natural Science Foundation of China (Grant no. 50571057), 863 High-Tech Research and Development Program of China (Grant no. 2006AA03Z339) and Shanghai Rising-Star Program (Grant no. 06QA14020). EZ acknowledges financial support by a European Union funded Marie Curie EST fellowship (Contract no. MEST-CT-2005-020986).

## References

[1] J.H. Perepezko, M.J. Uttormark, Undercooling and nucleation during solidification, ISIJ International 35 (6) (1995) 580–588.
[2] J.H. Perepezko, J.L. Sebright, P.G. Hockel, G. Wilde, Undercooling and solidification of atomized liquid droplets, Materials Science and Engineering A 326 (2002) 144–153.
[3] K.I. Dragnevski, A.M. Mullis, R.F. Cochrane, The effect of experimental variables on the levels of melt undercooling, Materials Science and Engineering A 375–377 (2004) 485–487.
[4] S.N. Ojha, Metastable phase formation during solidification of undercooled melt, Materials Science and Engineering A 304–306 (2001) 114–118.
[5] X.R. Liu, C.D. Cao, B. Wei, Microstructure evolution and solidification kinetics of undercooling Co–Ge eutectic alloys, Scripta Materialia 46 (2002) 13–18.
[6] Q.J. Zhai, Y.-L. Gao, W.B. Guan, Role of size and cooling rate in quenched droplet of SnBi eutectic alloy, Materials Science and Engineering A 441 (2006) 278–281.
[7] A.F. Lopeandia, J. Rodriguez-Viejo, Size-dependent melting and supercooling of Ge nanoparticles embedded in a $SiO_2$ thin film, Thermochimica Acta 461 (1–2) (2007) 82–87.
[8] Y.S. Kim, K.S. Kim, C.W. Hwang, K. Suganuma, Effect of composition and cooling rate on microstructure and tensile properties of Sn–Zn–Bi alloys, Journal of Alloys and Compounds 352 (1–2) (2003) 237–245.
[9] T. Mizoguchi, J.H. Perepezko, Nucleation behavior during solidification of casting iron at high undercooling, Materials Science and Engineering A 226 (1997) 813–817.
[10] B.A. Mueller, J.H. Perepezko, The undercooling of aluminium, Metallurgical and Materials Transactions A 18 (1987) 1143–1150.
[11] J.H. Perepezko, P.G. Höckel, J.S. Paik, Initial crystallization kinetics in undercooled droplets, Thermochimica Acta 388 (2002) 129–141.

[12] M.J. Uttormark, J.W. Zanter, H. Perepezko, Repeated nucleation in an undercooled aluminum droplet, Journal of Crystal Growth 177 (1997) 258–264.
[13] L.H. Allen, G. Ramanath, S.L. Lai, Z. Ma, S. Lee, D.D.J. Allman, K.P. Fuchs, 1000000 °C/S thin film electrical heater: in situ resistivity measurements of andl TilSi thin films during ultra rapid thermal annealing, Applied Physics Letters 64 (4) (1994) 417–419.
[14] Y. Efremov, E.A.Z.M. Olson, S.L. Lai, F. Schiettekatte, Z.S. Zhang, L.H. Allen, Thin-Film MEMS differential scanning nanocalorimetry: heat capacity analysis, Thermochimica Acta 412 (2004) 13–23.
[15] A.A. Minakov, C. Schick, Ultrafast thermal processing and nanocalorimetry at heating and cooling rates up to 1 MK/s, Review of Scientific Instruments 78 (7) (2007) 073902–073910.
[16] S.A. Adamovsky, A.A. Minakov, C. Schick, Scanning microcalorimetry at high cooling rate, Thermochimica Acta 403 (1) (2003) 55–63.
[17] A.F. Lopeandía, L.I. Cerdó, M.T. Clavaguera-Mora, L.R. Arana, K.F. Jensen, F.J. Muñoz, J. Rodríguez-Viejoa, Sensitive power compensated scanning calorimeter for analysis of phase transformations in small samples, Review of Scientific Instruments 76 (2005) 065104.
[18] A.F. Lopeandia, J. Valenzuela, J. Rodríguez-Viejo, Power compensated thin film calorimetry at fast heating rates, Sensors and Actuators A: Physical 143 (2) (2008) 256–264.
[19] M. Amagai, M. Watanabe, M. Omiya, K. Kishimoto, T. Shibuya, Mechanical characterization of Sn–Ag-based lead-free solders, Microelectronics Reliability 42 (2002) 951–966.
[20] M.F.J. Pijpers, V.B.F. Mathot, B. Goderis, R. Scherrenberg, E. van der Vegte, High-speed calorimetry for the analysis of kinetics of vitrification, crystallization and melting of macromolecule, Macromolecules 35 (9) (2002) 3601–3613.
[21] N.E. Hager, Thin heater calorimeter, Review of Scientific Instruments 35 (5) (1964) 618–624.
[22] M.Y. Efremov, E.A. Olson, M. Zhang, F. Schiettekatte, Z. Zhang, L.H. Allen, Ultrasensitive, fast, thin-film differential scanning calorimeter, Review of Scientific Instruments 75 (1) (2004) 179–191.
[23] A.A. Minakov, S.A. Adamovsky, C. Schick, Non adiabatic thin-film (chip) nanocalorimetry, Thermochimica Acta 432 (2) (2005) 177–185.
[24] A.W. van Herwaarden, Overview of calorimeter chips for various applications, Thermochimica Acta 432 (2) (2005) 192–201.
[25] A. Minakov, J. Morikawa, T. Hashimoto, H. Huth, C. Schick, Temperature distribution in a thin-film chip utilized for advanced nanocalorimetry, Measurement Science & Technology 17 (2006) 199–207.
[26] E. Zhuravlev, C. Schick, in preparation (2008).
[27] S. Neuenfeld, C. Schick, Verifying the symmetry of differential scanning calorimeters concerning heating and cooling using liquid crystal secondary temperature standards, Thermochimica Acta 446 (1–2) (2006) 55–65.
[28] M.J. O'Neill, The analysis of a temperature-controlled scanning calorimeter, Analytical Chemistry 36 (7) (1964) 1238–1245.
[29] E.S. Watson, M.O. O'Neill, J. Justin, N. Brenner, A differential scanning calorimeter for quantitative differential thermal analysis, Analytical Chemistry 36 (7) (1964) 1233–1238.
[30] X.Z. Xia, C.D. Zou, Y.-L. Gao, Preparation techniques and characterization for Sn–3.0Ag–0. 5Cu nanopowders, in: IEEE Proceedings of HDP'07, 2007, pp. 302–305.
[31] G.W.H. Hohne, H.K. Cammenga, W. Eysel, E. Gmelin, W. Hemminger, The temperature calibration of scanning calorimeters, Thermochimica Acta 160 (1) (1990) 1–12.
[32] W. Hemminger, G.W.H. Hohne, Calorimetry—Fundamentals and Practice, VCH, Weinheim, 1984.
[33] G. Wilde, J.L. Sebright, J.H. Perepezko, Bulk liquid undercooling and nucleation in gold, Acta Materialia 54 (2006) 4759–4769.
[34] S.M. Sarge, G.W.H. Hohne, H.K. Cammenga, W. Eysel, E. Gmelin, Temperature, heat and heat flow rate calibration of scanning calorimeters in the cooling mode, Thermochimica Acta 361 (2000) 1–20.
[35] B. Vinet, L. Cortella, Analysis of the different nucleation behaviour of tantalum samples processed in the Grenoble high drop tube, Materials Science and Engineering A 178 (1994) 125–128.